Analyses of intrinsic magnetoelectric properties in spin-valve-type tunnel junctions with high magnetoresistance and low resistance

Xiu-Feng Han,* Andrew C. C. Yu, Mikihiko Oogane, Junichirou Murai, Tadaomi Daibou, and Terunobu Miyazaki

Department of Applied Physics, Graduate School of Engineering, Tohoku University, Sendai 980-8579, Japan

(Received 4 October 2000; published 9 May 2001)

A series of experimental data was obtained systematically for a spin-valve-type tunnel junction of Ta (5 nm)/$Ni_{79}Fe_{21}$ (3 nm)/Cu (20 nm)/$Ni_{79}Fe_{21}$ (3 nm)/$Ir_{22}Mn_{78}$ (10 nm)/$Co_{75}Fe_{25}$ (4 nm)/Al (0.8 nm)-oxide/$Co_{75}Fe_{25}$ (4 nm)/$Ni_{79}Fe_{21}$ (20 nm)/Ta (5 nm). Analyses of (i) temperature dependence of tunnel magnetoresistance (TMR) ratio and resistance from 4.2 K to room temperature, (ii) applied dc bias-voltage dependence of TMR ratio and resistance at 6.0 K and room temperature, and (iii) tunnel current I and dynamic conductance (dI/dV) as functions of dc bias voltage at 6.0 K were carried out. High-TMR ratio of 64.7% at 4.2 K and 44.2% at room temperature were observed for this junction after annealing at 300 °C for an hour. An anisotropic wavelength cutoff energy of spin-wave spectrum in magnetic tunnel junctions, which is essential for self-consistent calculations, was suggested based on a series of inelastic electron tunnel spectra obtained. The main intrinsic magnetoelectric properties in such spin-valve-type tunnel junction with high magnetoresistance and low resistance can be evaluated based on the magnon-assisted inelastic excitation model and theory.

DOI: 10.1103/PhysRevB.63.224404 PACS number(s): 75.70.Ak, 73.40.Gk, 72.10.Di, 73.50.Bk

I. INTRODUCTION

Tunnel magnetoresistance (TMR) effect has attracted many researchers' attention[1–7] because this effect possesses a very high application potential in magnetic random access memory and magnetic-read-head technology.[8–13] Spin-electron transport and nanoscale magnetism in ferromagnet/insulator/ferromagnet (FM/I/FM) junction structure play a very important role in this field. Therefore, the TMR effect is a very interesting and useful research topic for both fundamental and applied physics. We believe that the very high density magnetic storage between 50 and 100 Gbit/inch^2 or even higher can be achieved based on the TMR effect together with the application of the submicrofabrication and nanofabrication techniques in the near future. It will be a widespread and profound influence to numerous fields of science and technology.

Up to present, although considerable progress on both experimental and theoretical studies of TMR effect in FM/I/FM junctions has been achieved, intrinsic magnetoelectric properties of magnetic tunnel junctions (MTJ's) as well as spin-electron transport theory have not yet been generally reported. Therefore, further investigations on these subjects are important, not only for the sake of fundamental studies, but also essential for the development of high-quality TMR devices.

In this article, the magnetoelectric properties of a typical spin-valve-type tunnel junction were selected for systematic analysis and discussion. TMR ratio of 64.7% obtained at 4.2 K [44.2% at room temperature (RT)] was very close to the expected value of the junction using $Co_{75}Fe_{25}$ ferromagnetic electrodes[14,15] and the resistance-area product was 3017 $\Omega\,\mu m^2$, which implies that defects in the Al-O barrier and at the interfaces between FM/I/FM layers are very few and the interface defects and impurity-assisted inelastic scattering can be neglected. Furthermore, the TMR model and theory developed by Zhang *et al.*[5] based on magnon emission or absorption by the tunneling electrons during the tunnel process was extended by defining an anisotropic-wavelength-cutoff energy of spin-wave spectrum in the MTJ's. Using this extended model, the magnetoelectric properties of the TMR junction can be explained and the calculation results are consistent with the experimental data.

II. EXPERIMENTAL METHOD

Spin-valve-type tunnel junctions with structure of Ta (5 nm)/$Ni_{79}Fe_{21}$ (3 nm)/Cu (20 nm)/$Ni_{79}Fe_{21}$ (3 nm)/$Ir_{22}Mn_{78}$ (10 nm)/$Co_{75}Fe_{25}$ (4 nm)/Al (0.8 nm)-oxide/$Co_{75}Fe_{25}$ (4 nm)/$Ni_{79}Fe_{21}$ (20 nm)/Ta (5 nm) were fabricated using sputter deposition and patterned using microfabrication technique followed by optimum heat treatment. Detailed description was reported in our previous works.[14] The effective barrier height ϕ and width d were obtained by fitting the current I vs dc bias voltage V curves to Simmons's equation with an asymmetric potential barrier in the insulating layer between the top and bottom magnetic electrodes.[16,17]

III. THEORETICAL METHOD

According to the model and theory developed by Zhang *et al.*[5] the conductance $G=I/V$ at zero voltage and zero temperature is denoted as G_0^γ, where $\gamma=(\mathrm{P,AP})$ represents the parallel (P) and antiparallel (AP) alignments of the magnetization of the two FM electrodes. The added components for the bias voltage and temperature dependence are indicated as $\Delta G_V^\gamma(V)$ and $\Delta G_T^\gamma(T)$, respectively. Considering a simple case for two identical FM electrodes, the conductance at 0 K and zero bias can be written respectively as

$$G_{V,T=0}^\gamma(V)=G_0^\gamma(0)+\Delta G_V^\gamma(V), \tag{1}$$

$$G_{T,V=0}^\gamma(T)=G_0^\gamma(0)+\Delta G_T^\gamma(T), \tag{2}$$

 ©2001 The American Physical Society

where

$$G_0^\gamma(0) = \frac{4\pi e^2}{\hbar}[|T^d|^2 + 2S^2|T^J|^2]A^\gamma, \tag{3}$$

$$\Delta G_V^\gamma(V) = \frac{4\pi e^2}{\hbar}|T^J|^2 B^\gamma \nu(V), \tag{4}$$

$$\Delta G_T^\gamma(T) = \frac{4\pi e^2}{\hbar}\frac{2Sk_BT}{E_m}|T^J|^2 B^\gamma \tau(T), \tag{5}$$

and

$$A^\gamma = \begin{cases} \rho_M^2 + \rho_m^2, & \text{when } \gamma = \text{P}, \\ 2\rho_M\rho_m, & \text{when } \gamma = \text{AP}. \end{cases} \tag{6}$$

$$B^\gamma = \begin{cases} 2\rho_M\rho_m, & \text{when } \gamma = \text{P}, \\ \rho_M^2 + \rho_m^2, & \text{when } \gamma = \text{AP}. \end{cases} \tag{7}$$

$$\nu(V) = \begin{cases} \text{SeV}/E_m, & \text{for } eV < E_m, \\ S(2 - E_m/eV), & \text{for } eV > E_m. \end{cases} \tag{8}$$

$$\tau(T) = -\ln[1 - e^{-E_c^\gamma/k_BT}] = \ln\left(\frac{k_BT}{E_c^\gamma}\right), \quad \text{for } k_BT > E_c^\gamma. \tag{9}$$

The definitions of all the parameters and subfunctions mentioned above can be referred to Ref. 5. An anisotropic-wavelength-cutoff energy of spin-wave spectrum E_c^γ with two different values representing the parallel and antiparallel configurations is introduced in this work for the following two reasons. First, a sharp peak in the inelastic electron tunneling (IET) spectrum, i.e., d^2I/dV^2 vs V, can usually be observed in good TMR junctions at a low bias voltage, which corresponds to the maximum probability (MP) energy of magnon-collective excitations E_{MP} of local spins at the interface between the insulating barrier and the FM electrodes. The E_{MP} for AP alignment is always larger than that for P alignment for the MTJ.[18] It is shown that the E_{MP} is anisotropic for AP and P alignments, i.e., $E_{\text{MP}}^{\text{AP}} > E_{\text{MP}}^{\text{P}}$. It was also confirmed by the tunneling spectra of single-crystal Fe/Al_2O_3/FeCo, i.e., Fe(100)/Al_2O_3/FeCo, Fe(211)/Al_2O_3/FeCo, and Fe(110)/Al_2O_3/FeCo, and the tunneling spectra of magnetically parallel and antiparallel configurations for Fe(100)/Al_2O_3/FeCo at 2 K.[19] For example, two peaks were observed at around 19.5 ± 1.0 mV for AP and 5.8 ± 1.0 mV for P alignment in Ta(5 nm)/$Ni_{79}Fe_{21}$(25 nm)/$Ir_{22}Mn_{78}$(12 nm)/$Co_{75}Fe_{25}$(4 nm)/Al(0.8 nm)-oxide/$Co_{75}Fe_{25}$(4 nm)/$Ni_{79}Fe_{21}$(25 nm)/Ta(5 nm) junction's IET spectrum at 4.2 K as that shown in Fig. 1. The P configuration in Fig. 1 was measured under magnetic field of -100 Oe, the AP configuration was achieved by increasing the field to 430 Oe then decreasing to 100 Oe. The sign of the magnetic field is relative to the field direction applied during sample deposition. The value of d^2I/dV^2 increased rapidly with increasing bias voltage from 0 to 4.0 mV, which suggests that the magnon excitations can occur at a very small bias voltage even less than 1.0 mV, which implies that the wavelength-cutoff energy of spin-wave spectrum, E_c, in such MTJ's is very small (between 0 and 1.0 meV). It can be suggested that the E_c is also anisotropic for AP and P alignments and $E_c^{\text{AP}} > E_c^{\text{P}}$ based on the larger difference between the E_{MP}^γ for AP and P alignments. Another clear peak of Al-O phonon was observed between 90 and 100 mV in such IET spectrum, which suggests that the emission and absorption of phonon-assisted tunneling process should be considered in quantitative calculation when the bias voltage is higher than 90 mV. The second reason for the difference in E_c^γ is that such an anisotropic E_c^γ is essential for calculating the magnetoelectric properties for the same TMR junction using one set of parameters. The temperature dependence of the resistances R^{AP} and R^{P} with AP and P alignment configurations from 4.2 to 300 K at 1.0 mV bias voltage cannot be calculated self-consistently using Eqs. (18) and (19) as shown below if $E_c^{\text{AP}} = E_c^{\text{P}}$ (i.e., if when E_c is isotropic). It can be seen later that the difference between the temperature dependence of the resistances R^{AP} and R^{P} is resulting from the difference between E_c^{AP} and E_c^{P}, besides the contributions of $1/\xi$ and ξ in Eqs. (18) and (19). However, normalized conductance can be deduced from Eqs. (1)–(5) as follows:

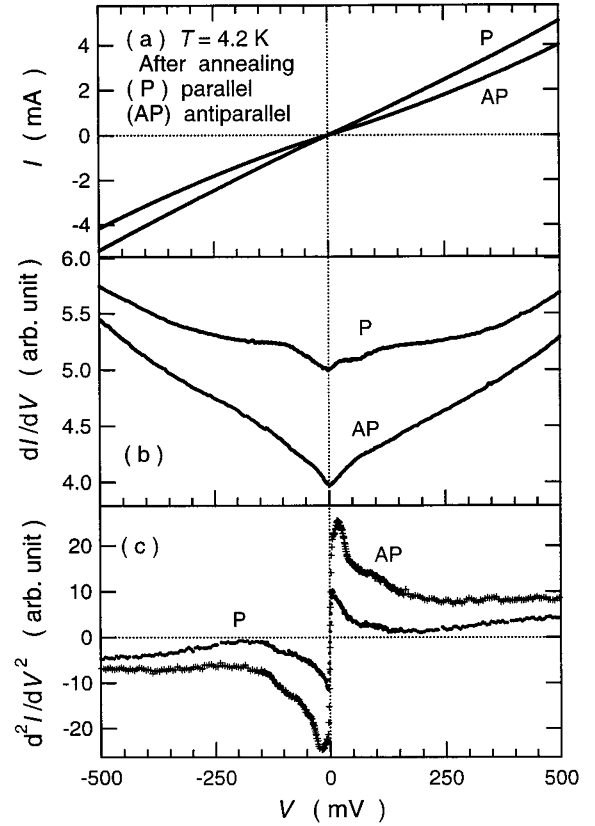

FIG. 1. (a) Tunnel current I and (b) dynamic conductance dI/dV as functions of dc bias voltage at 4.2 K for the junction Ta(5 nm)/$Ni_{79}Fe_{21}$(25 nm)/$Ir_{22}Mn_{78}$(12 nm)/$Co_{75}Fe_{25}$(4 nm)/Al(0.8 nm)-oxide/$Co_{75}Fe_{25}$(4 nm)/$Ni_{79}Fe_{21}$(25 nm)/Ta(5 nm) after annealing at 250 °C for an hour. (c) IET spectrum, d^2I/dV^2 vs V, at 4.2 K for the same MTJ.

$$\frac{G^{\gamma}_{V,T=0}(V)}{G^{\gamma}_{0}(0)}=1+QC^{\gamma}\nu(V), \tag{10}$$

$$\frac{G^{\gamma}_{T,V=0}(T)}{G^{\gamma}_{0}(0)}=1+QC^{\gamma}\frac{2Sk_BT}{E_m}\tau(T), \tag{11}$$

where

$$Q=\frac{1}{|T^d|^2/|T^J|^2+2S^2}, \tag{12}$$

$$C^{\gamma}=B^{\gamma}/A^{\gamma}=\begin{cases}\xi, & \text{when } \gamma=\text{P},\\ 1/\xi, & \text{when } \gamma=\text{AP},\end{cases} \tag{13}$$

$$\text{and } \xi=\frac{2\rho_M\rho_m}{\rho_M^2+\rho_m^2}=\frac{2}{\rho_M/\rho_m+\rho_m/\rho_M}. \tag{14}$$

The bias voltage or temperature dependence of the normalized resistance can be easily deduced from Eq. (10) and Eq. (11) by the reciprocal transformation between the conductance and resistance. Therefore, the bias voltage dependence of the resistances can be given by

$$\frac{R^{\gamma}_{V,T=0}(V)}{R^{\gamma}_{0}(0)}=\begin{cases}\dfrac{1}{1+QC^{\gamma}(SeV/E_m)}, & \text{for } eV<E_m,\\[2ex] \dfrac{1}{1+QC^{\gamma}S(2-E_m/eV)}, & \text{for } eV>E_m.\end{cases} \tag{15}$$

When $eV \ll E_m$, that is $QSeV/\xi E_m \ll 1$, the bias voltage dependence of TMR ratio can be deduced as follows:

$$\text{TMR}_{V,T=0}(V)=\frac{R^{\text{AP}}_{V,T=0}(V)-R^{\text{P}}_{V,T=0}(V)}{R^{\text{P}}_{V,T=0}(V)},$$

$$=\left(\frac{R^{\text{AP}}_0(0)}{R^{\text{P}}_0(0)}\right)\left[\frac{1+Q\xi(SeV/E_m)}{1+(Q/\xi)(SeV/E_m)}\right]-1, \tag{16}$$

$$\simeq \text{TMR}_{V,T=0}(0)-\frac{R^{\text{AP}}_0(0)}{R^{\text{P}}_0(0)}\left(\frac{1}{\xi}-\xi\right)\frac{Q\text{SeV}}{E_m}. \tag{17}$$

In which, $\text{TMR}_{V,T=0}(0)=[R^{\text{AP}}_0(0)-R^{\text{P}}_0(0)]/R^{\text{P}}_0(0)$ is the TMR ratio of the MTJ's at 0 K and 0 dc bias. It is determined by the effective barrier height ϕ and width d, and spin-polarization P of the two FM electrodes at 0 K and zero bias.[1,16,17]

When $k_BT>E^{\gamma}_c$, the temperature dependence of resistance and TMR ratio at zero bias can be deduced as follows:

$$R^{\text{AP}}_{T,V=0}(T)=\frac{R^{\text{AP}}_0(0)}{1+(Q/\xi)(2Sk_BT/E_m)\ln(k_BT/E^{\text{AP}}_c)}, \tag{18}$$

$$R^{\text{P}}_{T,V=0}(T)=\frac{R^{\text{P}}_0(0)}{1+Q\xi(2Sk_BT/E_m)\ln(k_BT/E^{P}_c)}, \tag{19}$$

and

$$TMR_{T,V=0}(T)=\frac{R^{\text{AP}}_{T,V=0}(T)-R^{\text{P}}_{T,V=0}(T)}{R^{\text{P}}_{T,V=0}(T)}$$

$$=\left(\frac{R^{\text{AP}}_0(0)}{R^{\text{P}}_0(0)}\right)\times\left[\frac{1+Q\xi(2Sk_BT/E_m)\ln(k_BT/E^{\text{P}}_c)}{1+(Q/\xi)(2Sk_BT/E_m)\ln(k_BT/E^{\text{AP}}_c)}\right]-1, \tag{20}$$

$$\simeq TMR_{T,V=0}(0)-\left(\frac{2QSk_BT}{E_m}\right)\left(\frac{R^{\text{AP}}_0(0)}{R^{\text{P}}_0(0)}\right)\times\left[\frac{1}{\xi}\ln\left(\frac{k_BT}{E^{\text{AP}}_c}\right)-\xi\ln\left(\frac{k_BT}{E^{\text{P}}_c}\right)\right]. \tag{21}$$

In that, $\text{TMR}_{T,V=0}(0)=\text{TMR}_{V,T=0}(0)=[R^{\text{AP}}_0(0)-R^{\text{P}}_0(0)]/R^{\text{P}}_0(0)$ is the TMR ratio of the MTJ's at 0 dc bias and 0 K.

IV. RESULTS AND DISCUSSION

In order to keep the same value of the matrix element ratio $|T^d|^2/|T^J|^2$ in Eq. (12) for calculating self-consistently the magnetoelectric properties of an MTJ using Eqs. (15)–(21), it is necessary to use the same MTJ for all the experimental data measurement. Experimental data presented in Figs. 2–6 were all measured using the same junction. Among them, results shown in Figs. 3–6 were measured on the same junction after annealing as that shown in Figs. 2(b), 2(c), and 2(d).

Figure 2 shows the TMR curves measured at RT, 77, and 4.2 K for the MTJ at its as-deposited state (a) and after annealing at 300 °C for an hour (b, c, and d). The junction area S is 5×5 μm^2. The experimental data in Fig. 2(a) was measured by a dc four-probe method with a dc bias of 1.0 mV and the others in Figs. 2(b), 2(c), and 2(d) were measured by a physical properties measurement system (PPMS; Model 6500, Quantum Design). The TMR ratio increased about two times from 23.7% [as-deposited state in Fig. 2(a)] to 44.2% after annealing as that shown in Fig. 2(b). A high TMR ratio of 64.7% was observed at 4.2 K, which was much higher than the 44.2%-RT TMR ratio. It was mainly due to the decrease of magnon excitations as well as the absence of phonon excitations. The effective barrier height ϕ, barrier width d, and resistance-area product R_S of the annealed MTJ were 2.21 eV, 0.78 nm, and 3017 $\Omega\,\mu$m^2, respectively, at 4.2 K. The effective barrier width d is close to the deposited Al thickness of 0.80 nm.

Figure 3 displays the TMR ratio and resistance R vs dc bias voltage curves measured at RT. The magnetic field for P configuration was chosen to be -1000 Oe. The data points

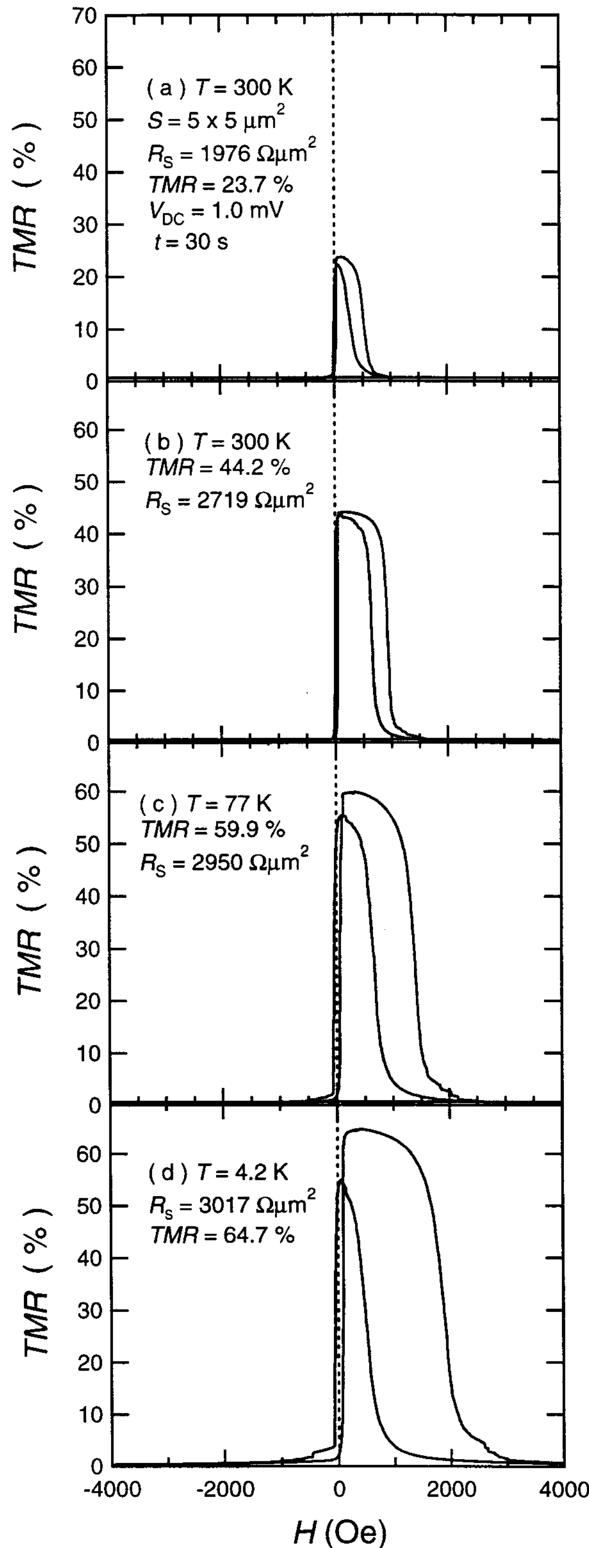

FIG. 2. TMR curves measured at RT, 77, and 4.2 K for the tunnel junction at the as-deposited state (a) and after annealing at 300 °C for an hour (b, c, and d).

for AP configuration were extracted from the TMR curves, which correspond to different magnetic fields that give optimal AP configuration. The half-peak widths in the TMR ratio vs dc bias voltage curves were about 410 and 500 mV

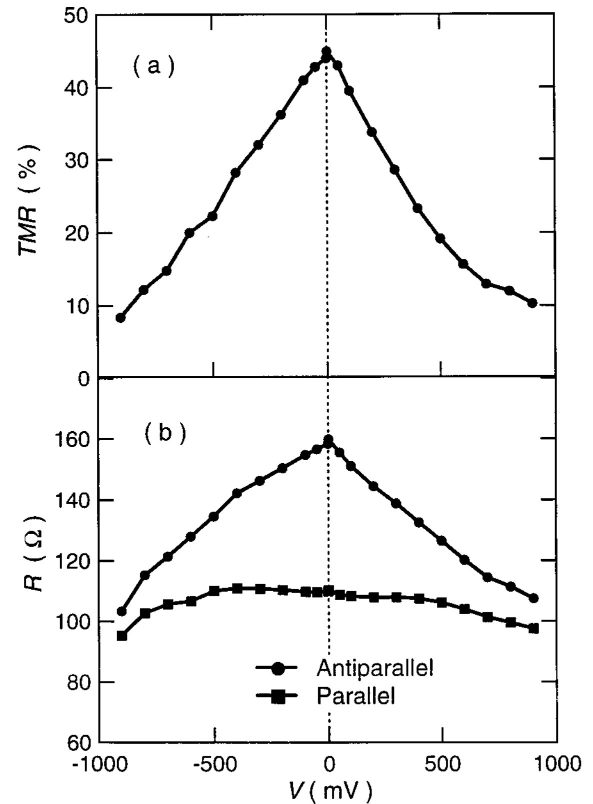

FIG. 3. TMR ratio and resistance R vs dc bias voltage curves measured at RT for the same junction as that shown in Fig. 1 after annealing.

when a positive and a negative dc bias voltage was applied, respectively.

Figure 4 shows the tunnel current I (a) and dynamic conductance dI/dV (b) as functions of the dc bias voltage measured by the PPMS at 6.0 K, using a few milliamperes dc current reduplicating 0.4 μA ac current when the magnetization of the two electrodes were in P and AP alignments, respectively. The increase of the current for AP alignment of the magnetization of the two electrodes was slower than that for P alignment as that shown in Fig. 4(a) due to the larger resistance of the AP configuration than that of the P configuration. The increase of conductance with increasing applied dc bias voltage was faster for AP alignment as shown in Fig. 4(b). It occurred because the increase of the conductance is proportional to $1/\xi$ for AP and to ξ for P alignment while $1/\xi$ is always larger than ξ as shown in Eqs. (10) and (14).

Figure 5 shows the dc bias-voltage dependence of TMR^{IV} $(V,T=6.0\,\mathrm{K})$ and TMR^{GV} $(V,T=6.0\,\mathrm{K})$ ratio from 0 to ± 200 mV for the TMR junction. TMR^{IV} was deduced from the I vs V curves in Fig. 4(a) and TMR^{GV} was deduced from the dI/dV vs V curves in Fig. 4(b). Here a few milliamperes of current, i.e., a low bias voltage from 0 to 200 mV, was applied to the junction at 6.0 K in order to avoid the temperature fluctuation due to its relatively small resistance of 120 Ω at 4.2 K to the cooling system of the PPMS thermostat. In principle, the values of TMR^{IV} $(V,T=\mathrm{const})$ and TMR^{GV} $(V,T=\mathrm{const})$ should be identical with that of TMR^{RH} $(V,T=\mathrm{const})$, which was directly deduced from the

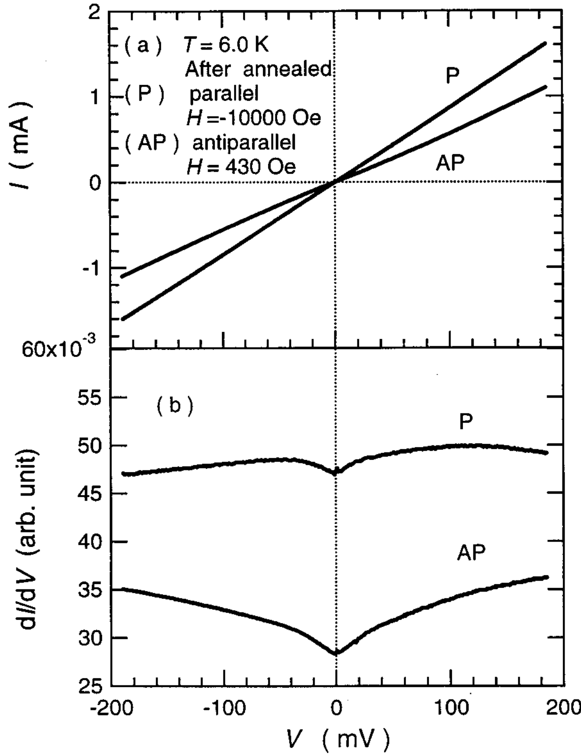

FIG. 4. Tunnel current I (a) and dynamic conductance dI/dV (b) as functions of the dc bias voltage at 6.0 K.

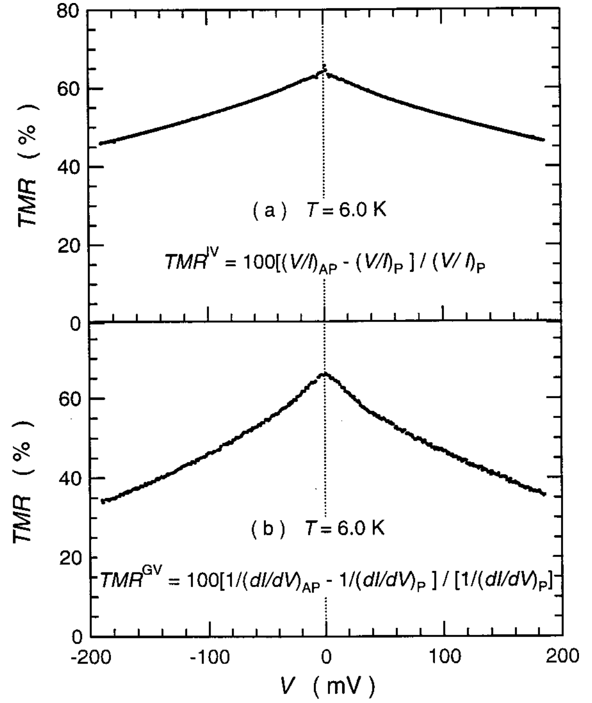

FIG. 5. dc-bias-voltage dependence of TMR^{IV} $(V,T=6.0\,\mathrm{K})$ and TMR^{GV} $(V,T=6.0\,\mathrm{K})$ ratio from 0 to ± 200 mV.

resistance R vs magnetic field H curve. In fact, it is shown in our measurement that

$$\mathrm{TMR}^{RH}(V,T=\mathrm{const})\simeq \mathrm{TMR}^{IV}(V,T=\mathrm{const}) > \mathrm{TMR}^{GV}(V,T=\mathrm{const}).$$

This is due to the restrictions of the bias voltage step ΔV. The exact values of TMR^{IV} $(V,T=\mathrm{const})$ and TMR^{GV} $(V,T=\mathrm{const})$ can only be achieved when $\Delta V\rightarrow 0$ during the measurement. However, when the bias-voltage step ΔV is too small, the measured signal will be very weak. Therefore, the value of TMR^{IV} $(V,T=\mathrm{const})$ is considered reliable comparing with that of TMR^{GV} $(V,T=\mathrm{const})$.

Figure 6 shows the temperature dependence of the TMR ratio, resistance, and coercivity from 4.2 to 300 K. The coercivity and optimal AP magnetic field for each data point was carefully deduced from TMR versus magnetic field (from $-10\,000$ to $10\,000$ Oe) curve at the specific temperature. Solid dots and squares are the experimental data and the solid lines represent the calculated values.

The intrinsic parameters, which were derived or extrapolated from experimental data, used for calculations are as follows: $R^{\mathrm{AP}}(0)=199.4\Omega$, $R^{\mathrm{P}}(0)=120.8\,\Omega$, $\mathrm{TMR}(0)=65.0\%$, the identical and effective spin-polarization of two FM electrodes $P=[\mathrm{TMR}(0)/(2+\mathrm{TMR}(0))]^{1/2}=49.5\%$, $\rho_M/\rho_m=(1+P)/(1-P)=2.96$, $\xi=0.606$, $1/\xi=1.65$, $S=3/2$, and $T_C=900\,^{\circ}\mathrm{C}$ for the $\mathrm{Co_{75}Fe_{25}}$ alloy, therefore $E_m=3k_BT_C/(S+1)=121$ meV.

The matrix element ratio $|T^d|^2/|T^J|^2=13.0$, i.e., $Q=0.0572$, can be first fitted into the dc-bias-voltage dependence of TMR ratio at 6.0 K (i.e., at near 0 K) from 0 to 80 mV using Eq. (16) or (17). Then E_c^{γ} can be fitted into the temperature dependence of the resistances for AP and P alignments from 4.2 to 300 K at 1.0 mV bias voltage (i.e., at near zero bias) using Eqs. (18) and (19), i.e., $E_c^{\mathrm{AP}}=0.260$ meV and $E_c^{\mathrm{P}}=0.164$ meV. Finally, these three fitting parameters, $|T^d|^2/|T^J|^2$, E_c^{AP}, and E_c^{P}, can be confirmed further by the calculation of the temperature dependence of TMR ratio from 4.2 to 300 K at 1.0 mV bias using Eq. (20) or (21).

It is reasonable that the value of $|T^d|$ is 1 to 2 orders of magnitude large than $|T^J|$ because $|T^d|$ is determined by overlapping the wave functions within the barrier while $|T^J|$ by the overlap of the wave function from one electrode at the barrier interface with the other electrode. From the energy point of view, $E_c^{\mathrm{AP}}=0.260$ meV, and $E_c^{\mathrm{P}}=0.164$ meV are corresponding to 3.0 and 1.9 K, respectively. This means that no magnon excitation occurs below such temperature for the AP and P alignments, respectively. Therefore, the TMR ratio can have the same value between 0 and 1.9 K. The value of $E_c=4.0$ meV that corresponds to 46.4 K, obtained by Zhang *et al.*,[5] is slightly large. The TMR ratio obviously decreased with increasing temperature from or even below 4.2 to 300 K, which suggests that the magnon excitations can occur starting from or even below 4.2 K, which corresponds to 0.362 meV. Therefore, the values of these three fitting parameters of $|T^d|^2/|T^J|^2$, E_c^{AP}, and E_c^{P} are reasonable. It is noticed that the E_c^{AP} and E_c^{P} are sensitive parameters for the temperature dependence of the resistances (conductance) and TMR ratio although they enter in the logarithm, and they

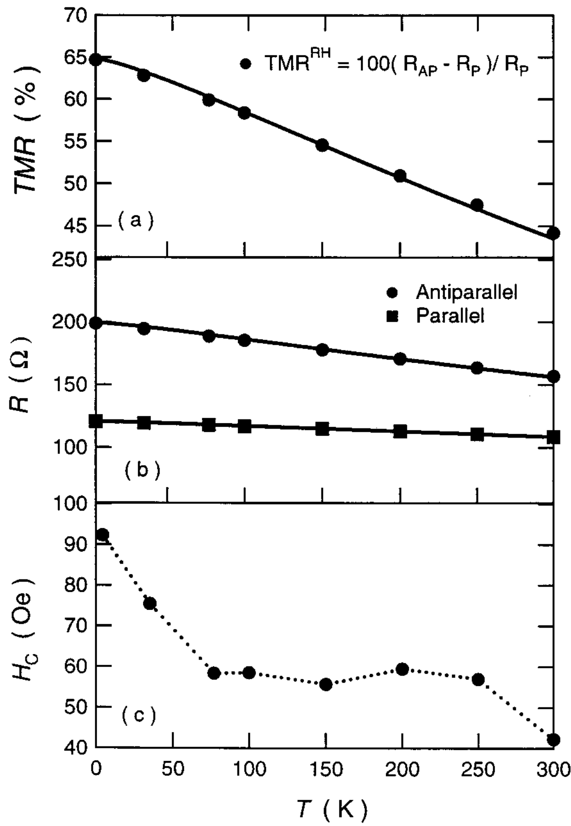

FIG. 6. Temperature dependence of the (a) TMR ratio, (b) resistances, and (c) coercivity from 4.2 K to RT. The solid dots and squares are the experimental data and the solid lines represent the calculated values.

need not vary with increasing temperature from 4.2 to 300 K in the self-consistent calculation.

Three resemble parameters, $|T^d|^2/|T^J|^2 = 13.0$, $E_c^{\mathrm{AP}} = 0.300\,\mathrm{meV}$, and $E_c^{\mathrm{P}} = 0.090\,\mathrm{meV}$, were obtained by using the similar calculation processes for another spin-valve-type junction as that shown in Ref. 14. It is noticed that the $|T^d|^2/|T^J|^2$ values are very close (here it is same for two junctions) for the junctions with the same layer structure. Therefore, it is believed that $|T^d|^2/|T^J|^2$ and E_c^{γ} are all the intrinsic parameters of the MTJ's.

An estimation on the origin of the anisotropic-cutoff energy E_c^{γ} in the different magnetic configurations is discussed in the text following. Let us consider that an external magnetic field $\mathbf{H}$ is applied to the *s-d* spin-electron system in the MTJ for the AP and P magnetic configurations in our experiment. In such case when an itinerant *s*-electron tunnels from one FM/I interface to the other I/FM interface, the itinerant *s* electron will change from one *s-d* exchange interaction state to the other. The Zeeman interaction Hamiltonian, $\mathbf{H}_m$, of the *s-d* electrons can be written as $\mathbf{H}_m = \mu_B \cdot \mathbf{H} + 2S\mu_B \cdot \mathbf{H}$ when we only consider the interaction terms that are related with the external magnetic field. In principle, the Zeeman energy together with the eigenvalues and eigenfunctions of the total perturbation Hamiltonian $\mathbf{H}_1$, which includes the Zeeman interaction $\mathbf{H}_m$, the *s-d* exchange interaction, and the *s*-electron–electric field interaction, etc., can be strictly evaluated by diagonalizing the matrix of perturbation Hamiltonian $\mathbf{H}_1$.[20] But the value of Zeeman energy for the *s-d* electrons can be simply estimated by using $\epsilon_m = 2(\mu_B H + 2S\mu_B H)$ with $S = 3/2$, in such an extreme case ϵ_m is the maximum Zeeman energy, when an itinerant *s*-electron tunnels from FM/I interface to the other one in an external magnetic field *H*. It was observed that an external magnetic field of about 2000 Oe was required to reverse the pinned FM layer from AP state to P state at 4.2 K as shown in Fig. 2(d). Therefore, the value of the maximum Zeeman energy for the *s-d* electrons was deduced as $\epsilon_m = 0.093\,\mathrm{meV}$ (which corresponds to 1.07 K). This estimated ϵ_m value is consistent with the value of the difference in two anisotropic cutoff energy, i.e., $E_c^{\mathrm{AP}} - E_c^{\mathrm{P}} = (0.260\text{-}0.164)\,\mathrm{meV} = 0.096\,\mathrm{meV}$ (which corresponds to 1.11 K). Therefore, the difference in the anisotropic-cutoff energy E_c^{γ} of magnon excitation can be interpreted as the difference in the energy gap between the ground and excited energy levels of the *s-d* electron system in the MTJ for AP and P magnetic configurations in our experiment. Such difference in the energy gap is mainly contributed by the Zeeman interaction and the *s-d* exchange interaction in an external magnetic field and/or in a demagnetization field.

In principle, the energy gap between the ground level and excited energy levels of the *s-d* electron system for AP and P magnetic configurations as well as the matrix-element ratio $|T^d|^2/|T^J|^2$ at 0 K and zero bias voltage for an MTJ with the three key layers of $\mathrm{Co_{75}Fe_{25}}(4\,\mathrm{nm})/\mathrm{Al}(0.8\,\mathrm{nm})$-oxide/$\mathrm{Co_{75}Fe_{25}}(4\,\mathrm{nm})$ can be evaluated using the electronic structure calculation method. Therefore, the parameters E_c^{γ} and $|T^d|^2/|T^J|^2$ obtained in this work supplied a useful criteria for the first-principle calculation in the MTJ's.

V. CONCLUSIONS

A spin-electron polarization tunneling model, based on magnon emission or absorption by the tunneling electrons during the tunnel process, was extended by defining an anisotropic-wavelength-cutoff energy of spin-wave. Such an anisotropic-wavelength-cutoff energy is smaller than 1.0 meV in these high-TMR junctions. Good intrinsic magnetoelectric properties, such as dc-bias-voltage dependence of TMR ratio and resistances near to 0 K between 0 and 80 mV and the temperature dependence of TMR ratio and resistances from 4.2 to 300 K at 1.0 mV bias can be self-consistently evaluated using this extended model and a unique set of intrinsic parameters. Therefore, it can help us to understand further the spin-electron transport and the inelastic magnon-scattering mechanism in MTJ's, ferromagnetic/nonmagnetic semiconductor and superconductor heterostructures, as well as ferromagnetically contacted carbon nanotubes.[13]

ACKNOWLEDGMENTS

This project was supported by Japan Society for the Promotion of Science (JSPS), Grant No. PD.98049 and in part by the Storage Research Consortium (SRC), NEDO Regional Consortium Project, and Grant-in-Aid for Scientific

Research (11355001 and 11792002) from the Ministry of Education, Science, Sports, and Culture in Japan. At the same time, X.-F. Han gratefully acknowledges the partial support of K. C. Wong Education Foundation (Hong Kong), National Key Laboratory of Theoretical and Computational Chemistry at Jilin University, and State Key Laboratory of Magnetism, Institute of Physics, Chinese Academy of Sciences.

*Author to whom correspondence should be addressed; email address: xiufenghan@hotmail.com

[1] M. Jullière, Phys. Lett. **54A**, 225 (1975).
[2] T. Miyazaki and N. Tezuka, J. Magn. Magn. Mater. **139**, L231 (1995).
[3] J. S. Moodera, L. R. Kinder, T. M. Wong, and R. Meservey, Phys. Rev. Lett. **74**, 3273 (1995).
[4] J. C. Slonczewski, J. Magn. Magn. Mater. **159**, L1 (1996).
[5] S. Zhang, P. M. Levy, A. C. Marley, and S. S. P. Parkin, Phys. Rev. Lett. **79**, 3744 (1997).
[6] S. T. Chui, Phys. Rev. B **74**, 5600 (1997).
[7] A. M. Bratkovsky, Appl. Phys. Lett. **72**, 2334 (1998).
[8] M. Sato and K. Kobayashi, IEEE Trans. Magn. **33**, 3553 (1997).
[9] J. M. Daughton, J. Appl. Phys. **81**, 3758 (1997).
[10] W. J. Gallagher, S. S. P. Pakin, Y. Lu, X. P. Bian, A. Marley, K. P. Roche, R. A. Altman, S. A. Rishton, C. Jahnes, T. M. Shaw, and G. Xiao, J. Appl. Phys. **81**, 3741 (1997).
[11] R. C. Sousa, J. J. Sun, V. Soares, P. P. Freitas, A. Kling, M. F. da Silva, and J. C. Soares, Appl. Phys. Lett. **73**, 3288 (1998).
[12] S. Tehrani, E. Chen, M. Durlam, M. Deherrera, J. M. Slaughter, J. Shi, and G. Kerszykowski, J. Appl. Phys. **85**, 5822 (1999).
[13] K. Tsukagoshi, B. W. Alphenaar, and H. Ago, Nature (London) **401**, 572 (1999).
[14] X. F. Han, M. Oogane, H. Kubota, Y. Ando, and T. Miyazaki, Appl. Phys. Lett. **77**, 283 (2000).
[15] D. J. Monsma and S. S. P. Parkin, Appl. Phys. Lett. **77**, 720 (2000).
[16] John G. Simmons, J. Appl. Phys. **34**, 1793 (1963).
[17] W. F. Brinkman, R. C. Dynes, and J. M. Rowell, J. Appl. Phys. **41**, 1915 (1970).
[18] J. Murai, Y. Ando, M. Kamijo, H. Kubota, and T. Miyazaki, Jpn. J. Appl. Phys., Part 2 **38**, L1106 (2000).
[19] T. Nagahama, Y. Suzuki, S. Yuasa, and E. Tamura, *Symposium of the 24th Annual Conference on Magnetics in Japan, Tokyo, 2000*, p. 38 (unpublished).
[20] X. F. Han, H. M. Jin, Z. J. Wang, T. S. Zhao, and C. C. Sun, Phys. Rev. B **47**, 3248 (1993).